

# Determining cooling rates from mica $^{40}\text{Ar}/^{39}\text{Ar}$ thermochronology data: effect of cooling path shape

C. S. McDonald<sup>1,2</sup>, C. J. Warren<sup>1\*</sup>, F. Hanke<sup>3</sup> and J. Chard<sup>4</sup>

<sup>1</sup>School of Environment, Earth and Ecosystem Sciences, The Open University, Walton Hall, Milton Keynes, MK7 6AA, United Kingdom

<sup>2</sup>School for Earth and Space Exploration, Arizona State University, BOX 876004, Tempe, Arizona, 85287-6004

<sup>3</sup>Dassault Systèmes, 334 Cambridge Science Park, Milton Road, Cambridge, CB4 0WN, United Kingdom

<sup>4</sup>School of Earth and Planetary Sciences, The Institute for Geoscience Research (TIGeR), Curtin University, Perth, WA 6845, Australia

\*clare.warren@open.ac.uk

*Keywords: Thermochronology, Diffusion Modelling, Closure Temperature, muscovite, biotite, rutile,  $^{40}\text{Ar}/^{39}\text{Ar}$ , U-Pb*

## Abstract

Tectonic models are commonly underpinned by metamorphic cooling rates derived from diffusive-loss thermochronology data. Such cooling ages are usually linked to temperature via Dodson's 1973 closure temperature ( $T_C$ ) formulation, which specifies a 1/time-shaped cooling path. Geologists, however, commonly discuss cooling rates as a linear temperature/time shape. We present the results of a series of simple finite-difference diffusion models for Ar diffusion in muscovite and biotite that show that the difference in recorded age between 1/t and linear cooling paths increases significantly with hotter starting temperatures, slower cooling rates and smaller grain sizes. Our results show that it is essential to constrain the cooling path shape in order to make meaningful interpretations of the measured data.

## Introduction

34 The ratio of parent to daughter radiogenic isotopes has been used for over a hundred  
 35 years to constrain geological ages and timescales (e.g. as reviewed by Condon and Schmitz,  
 36 2013). Minerals that host the radioactive parent element are commonly referred to as either  
 37 “geochronometers”, which record the timing of their crystallisation or “thermochronometers”,  
 38 which record the timing of cooling through an estimated temperature window at some point  
 39 after their crystallisation (e.g. as reviewed by Reiners, 2005). The record of different time-  
 40 temperature pairs in any one rock or tectonic region helps to constrain thermal history and thus  
 41 provide clues about the mechanism(s) by which the rocks were exhumed to the surface.

42 Many thermochronometers are based on the premise that some of the daughter isotope  
 43 concentration is lost via thermally-activated diffusion at high temperatures, and that the  
 44 resulting mineral age can be linked to temperature via the mathematics governing such  
 45 diffusion. The temperature of a thermochronometer-bearing rock at the time the  
 46 thermochronometer recorded its apparent (bulk, whole-grain average) cooling age is most  
 47 commonly estimated using Dodson’s closure temperature ( $T_C$ ) formulation (Dodson 1973),  
 48 which, for thermally activated diffusion described by

$$49 \quad D = D_0 e^{-E_a/RT} \quad [1]$$

50 is given by:

$$51 \quad T_C = R/[E_a \ln(A\tau D_0/a^2)] \quad [2]$$

52 Where  $D$  is the diffusion coefficient,  $D_0$  is the diffusion pre-exponential factor,  $R$  is the  
 53 gas constant,  $E_a$  is the activation energy,  $a$  is the diffusion (or grain) radius,  $A$  is a grain-shape-  
 54 related constant and  $\tau$  relates the  $T_C$  to cooling rate:

$$55 \quad \tau = \frac{R}{(E_a dT^{-1}/dt)} = - \frac{RT^2}{(E_a dT/dt)} \quad [3]$$

56 This result of an analytical solution to the diffusion equation has had an enduring legacy  
 57 due to its mathematical elegance and simplicity of application. However the Dodson  $T_C$   
 58 formulation is underpinned by several important assumptions and approximations:

59 (1) that thermally activated volume diffusion was the only mechanism by which the  
 60 daughter isotope was mobilised within the mineral;

61 (2) that the mineral crystallized with no inherited daughter isotope;

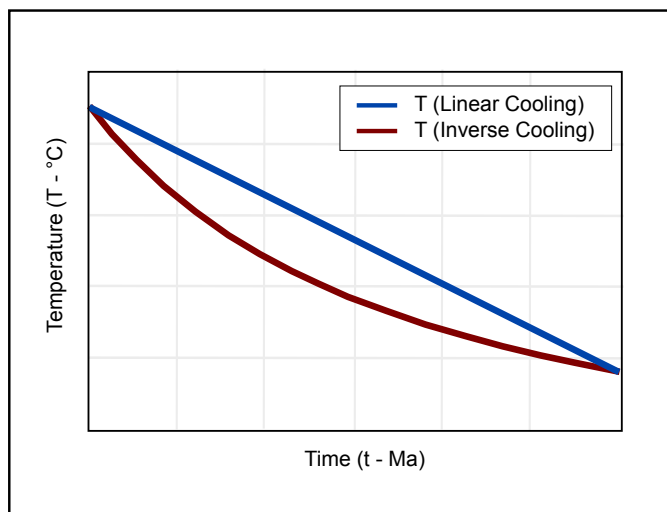
62 (3) that a daughter isotope concentration of zero was maintained at the mineral grain  
 63 boundary throughout cooling;

64 (4) that the starting temperature was high enough for diffusion of the daughter isotope  
 65 to be efficient, and removal from the grain to be geologically instantaneous, and

66 (5) that the cooling path from the time of crystallisation to the time of closure  
 67 conformed to a  $1/t$  (time) -shape.

68 These approximations have a major impact on the applicability of the formulation to  
69 any particular geological scenario. The further any scenario deviates from these assumptions,  
70 the greater the (commonly un-quantified and un-reported) interpretational uncertainties on the  
71 link between age and temperature. A refinement of the  $T_C$  formulation to consider cases that  
72 did not conform to point (4) was proposed by Ganguly and Tirone, 1999, but has not been  
73 applied by the thermochronometer community to nearly the same extent that the original  
74 Dodson formulation has been.

75 The Dodson closure temperature formulation is most commonly used to constrain  
76 cooling rates by linking the  $T_C$  + time pair to a higher temperature + time pair linearly.  
77 However,  $T_C$  has been derived explicitly for temperature histories that involve cooling  
78 proportional to  $1/t$  (Figure 1) as this creates a linear time dependence in the exponent in  $\exp(-$   
79  $E_a/RT)$  and allows the analytic integration of the time dependence. To calculate a closure  
80 temperature using the Dodson  $T_C$  formulation and then to use that result to calculate a linear  
81 cooling rate is therefore both circular (as also noted by e.g. Ganguly and Tirone, 2009) and  
82 ultimately incorrect.



83

84 **Fig. 1.** A schematic representation showing the difference between linear (blue) and  
85  $1/t$  (red) cooling paths. Note that the  $1/t$ -shaped path initially cools faster, therefore reducing  
86 the opportunity for daughter product loss by diffusion.

87

88 Modern analytical equipment can now provide ever more precise isotope concentration  
89 (age) data, at ever increasing spatial resolution. Furthermore, the diffusion equation can be  
90 solved numerically on any standard computer. Here we investigate the effects of linear and  $1/t$   
91 cooling path shapes on the bulk ages and core-rim age profiles of Ar in muscovite and biotite  
92 in grains of different radius that have cooled from different temperatures at different rates. The

93 model results show that the ages recorded by muscovite and biotite that have cooled following  
94 these different simple end-member paths differ significantly, especially at higher peak  
95 temperatures increase and smaller grain sizes. The results also allow cooling rates to be  
96 determined directly if there is independent evidence for cooling path shape, so long as the time  
97 at which cooling started is known.

98  
99

### 100 **The DiffArgP\_inverse Code**

101 The finite-difference code DiffArgP\_inverse is a modified version of DiffArg (Wheeler  
102 1996). It is written in Matlab 4.1 and solves the diffusion equation numerically.  
103 DiffArgP\_inverse differs from DiffArg in that it includes the effect of pressure on the diffusion  
104 of Ar in muscovite (Harrison et al., 2009) and the functionality to model 1/t-shaped thermal  
105 histories to match the analytical solution of Dodson, 1973, rather than only linear or piecewise-  
106 linear histories. DiffArg and its modified variants has previously been used to model Ar  
107 diffusion in different minerals that experienced complex metamorphic histories in a variety of  
108 tectonic environments (e.g. Mark et al., 2008; Warren et al., 2012a;b; Wartho et al., 2013;  
109 McDonald et al., 2016; 2018). The code allows the user to input any thermal and  
110 (de)compression history and produces outputs of integrated single grain (bulk) ages and core-  
111 rim age profiles. Any of the DiffArg versions are available from Hanke or Warren on request.  
112 Further details of the DiffArg\_Inverse code are presented in Supplementary Document S1.

113

### 114 **Methods**

115 The bulk (volume-integrated)  $^{40}\text{Ar}/^{39}\text{Ar}$  ages of muscovite and biotite of different grain  
116 size were modelled for a variety of different starting temperatures and linear vs. inverse (1/t)  
117 cooling histories. Muscovite and biotite were modelled with cylindrical geometry and grain  
118 radii of 1 mm, 0.5 mm, and 0.25 mm as these are the most typical grain sizes picked for  
119 metamorphic  $^{40}\text{Ar}/^{39}\text{Ar}$  analyses. The diffusion parameters applied to each mineral are outlined  
120 in Table 1.

121 All minerals were modelled as “crystallising” then instantaneously cooling from  
122 starting temperatures of 700°C, 600°C, 500°C, and 450°C at a starting pressure of 1 GPa to  
123 represent a variety of metamorphic terranes exhuming from mid-crustal conditions (Tables 1,  
124 2, 4, Supplementary Tables S.2, S.4). A series of muscovite models was run at a starting  
125 pressure of 2 GPa to more closely match conditions found in subduction zones (c.f. Warren et  
126 al., 2012a; Table 3, Supplementary Table S.3), and a further series of muscovite models was  
127 run with spherical geometry to allow comparison with the cylindrical geometry models

128 (Supplementary Table S.5 and Figure S.6). Linear cooling rates of 5, 10, 25, 50, and 70°CMa<sup>-1</sup>  
 129 were run in order to compare results for typical rates of cooling in different tectonic terranes.  
 130 1/t cooling rate models were run for equivalent “time to reach 0°C” as the linear models, in  
 131 order to compare results for different cooling path shapes. Model pressures were decreased to  
 132 0 GPa over the same time interval.

133 The grain boundary conditions in all models were modelled as zero daughter element  
 134 concentration, for the purposes of investigating behaviour in an open system. Model ages were  
 135 calculated for 2-dimensional (cylindrical) diffusion geometry (Hames and Bowring 1994) and  
 136 the time integration was performed using the Crank–Nicholson solver, with a recommended  
 137 time step that is 10 times larger than the value suggested for a stable fully-explicit method  
 138 (Table 1; Wheeler 1996).

139 A series of models was run to test the effect of the published experimental uncertainties  
 140 on E<sub>a</sub> and D<sub>0</sub> (Harrison et al., 2009 for muscovite and Harrison et al., 1985 for biotite) on the  
 141 model results. The results are detailed in Supplementary Table S.7.

142

143 **Table 1.** Diffusion and other model parameters used in this study.

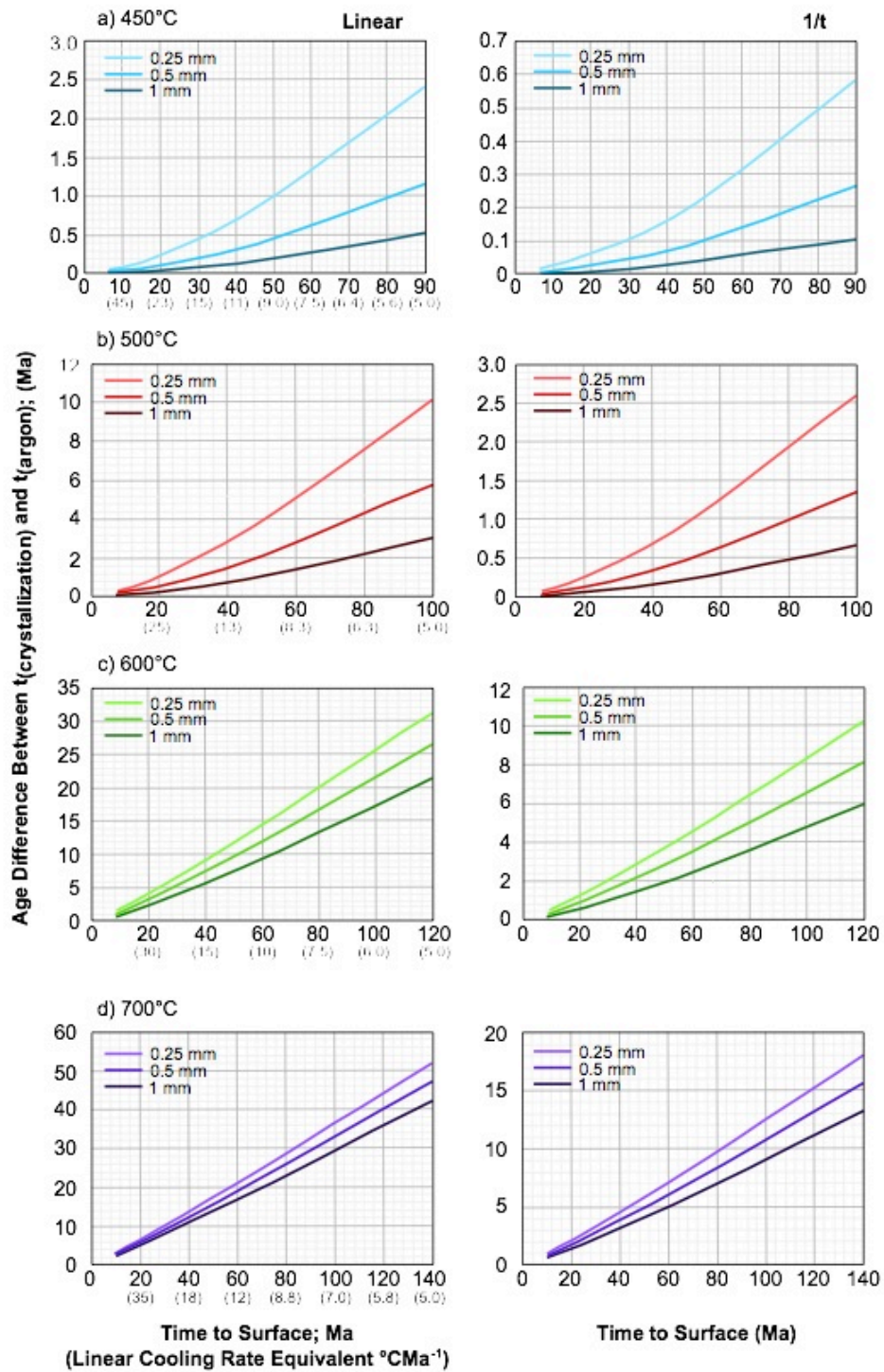
144

<b>Modelled diffusion parameters</b>						
<b>Mineral</b>	<b>System</b>	<b>E<sub>a</sub></b> Jmol <sup>-1</sup>	<b>D<sub>0</sub></b> mm <sup>2</sup> s <sup>-1</sup>	<b>V<sub>0</sub></b> cm <sup>3</sup> mol <sup>-1</sup>	<b>P<sub>0</sub></b> Gpa	<b>Reference</b>
Muscovite	<sup>40</sup> Ar/ <sup>39</sup> Ar	263592	2.30E+02	14	1	Harrison et al., (2009)
Biotite	<sup>40</sup> Ar/ <sup>39</sup> Ar	196648	7.70E+00	0	0	Harrison et al., (1985)
<b>Other model parameters</b>						
<b>Mineral</b>	<b>System</b>	<b>Grain shape</b>	<b>Radius range</b> mm	<b>Starting temp range</b> °C	<b>Linear cooling rate range</b> °C/Ma	<b>Starting pressure range</b> GPa
Muscovite	<sup>40</sup> Ar/ <sup>39</sup> Ar	Cylinder	1-0.25	700-450	5, 10, 25, 50, 70	2-1
Biotite	<sup>40</sup> Ar/ <sup>39</sup> Ar	Cylinder	1-0.25	700-450	5, 10, 25, 50, 70	1
<b>Global model parameters</b>						
Grain boundary:		Zero concentration				
Solver:		Crank-Nicholson				
Time step		10				

145

146           **Results**

147           The model results are plotted in Figures 2 and 3 (Muscovite modelled from pressures  
148 of 1 GPa and 2 GPa respectively) and 4 (Biotite from 1 GPa). Summary model results for the  
149 bulk (volume-averaged) ages are presented in Tables 2 (Muscovite), and 3 (Biotite). Full results  
150 including core-rim model age variations are presented in Supplementary Tables S.2 (Muscovite  
151 1 GPa) Table S.3 (Muscovite 2 GPa), Table S.4 (Biotite) and Table S.5 (Muscovite 1 GPa with  
152 spherical geometry).



153

154

155

156

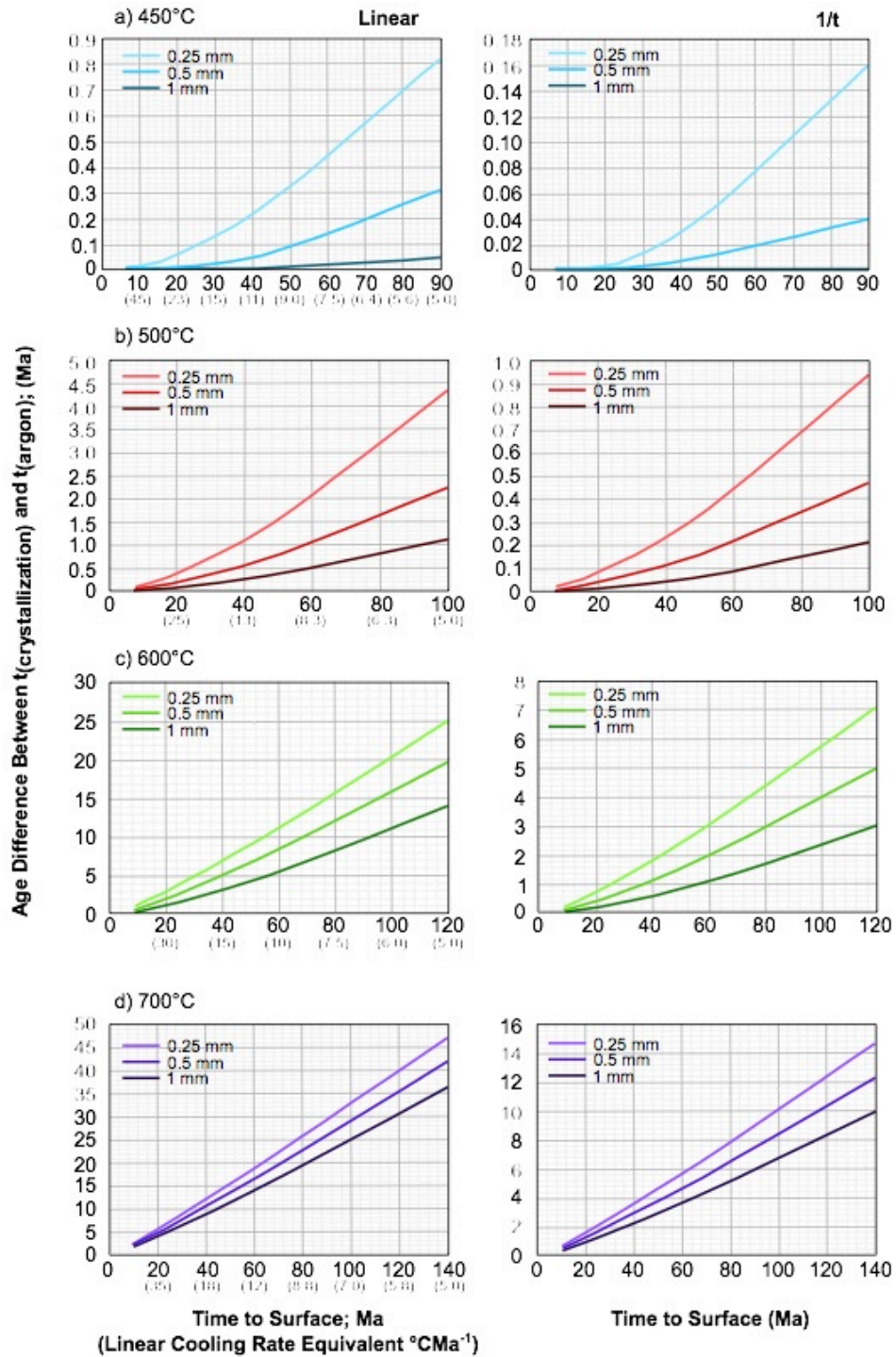
157

158

**Fig. 2.** Muscovite linear and 1/t results for models run at 1 GPa. Different coloured lines show different grain sizes. A-D show results for linear models at different starting temperatures; E-H show results for 1/t models that run over the same timescale. For ease of comparison, both sets of models run for the equivalent “time to surface” which is plotted on the x-axis. The equivalent linear rate is plotted underneath the “time to surface” value on the

159 *linear model plots. The y-axis plots the difference between the time at which cooling starts and*  
160 *the recorded  $^{40}\text{Ar}/^{39}\text{Ar}$  age: if this is, the grain size and the starting temperature are known for*  
161 *the analysed samples, then the cooling rate can be read off the graph directly. Note the*  
162 *differences in the y-axis scale between the linear and  $1/t$  results. The grey outline maps the*  
163 *maximum uncertainty associated with the experimental diffusion parameters of Harrison et al.,*  
164 *2009 for the 0.5 mm grain-size models (the results for the other grain sizes will scale*  
165 *accordingly).*

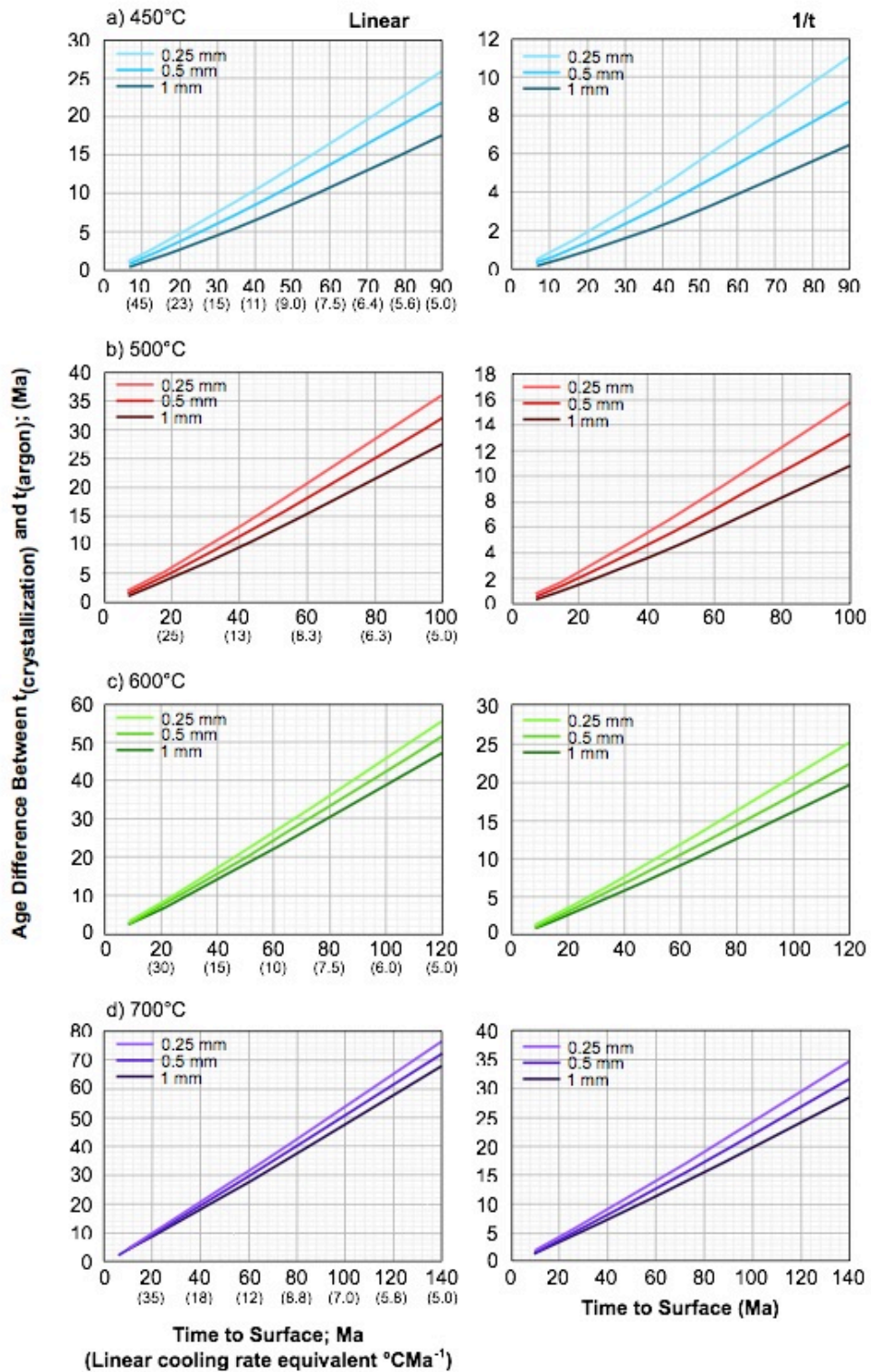




166  
 167  
 168  
 169  
 170  
 171  
 172

**Fig 3.** Muscovite linear and 1/t results for models run at 2 GPa. Different coloured lines show different grain sizes. A-D show results for linear models at different starting temperatures; E-H show results for 1/t models that run over the same timescale. For ease of comparison, both sets of models run for the equivalent “time to surface” which is plotted on the x-axis. The equivalent linear rate is plotted underneath the “time to surface” value on the linear model plots. The y-axis plots the difference between the time at which cooling starts and

173 *the recorded  $^{40}\text{Ar}/^{39}\text{Ar}$  age: if this is, the grain size and the starting temperature are known for*  
174 *the analysed samples, then the cooling rate can be read off the graph directly. Note the*  
175 *differences in the y-axis scale between the linear and  $1/t$  results. The grey outline maps the*  
176 *maximum uncertainty associated with the experimental diffusion parameters of Harrison et al.,*  
177 *2009 for the 0.5 mm grain-size models (the results for the other grain sizes will scale*  
178 *accordingly).*  
179



180

181

182

183

184

185

**Fig. 4.** Biotite linear and 1/t model results. Different coloured lines show different grain sizes. A-D show results for linear models at different starting temperatures; E-H show results for 1/t models that run over the same timescale. For ease of comparison, both sets of models run for the equivalent “time to surface” which is plotted on the x-axis. The equivalent linear rate is plotted underneath the “time to surface” value on the linear model plots. The y-axis

186 *plots the difference between the time at which cooling starts and the recorded  $^{40}\text{Ar}/^{39}\text{Ar}$  age: if*  
 187 *this is, the grain size and the starting temperature are known for the analysed samples, then*  
 188 *the cooling rate can be read off the graph directly. Note the differences in the y-axis scale*  
 189 *between the linear and 1/t results. The grey outline maps the maximum uncertainty associated*  
 190 *with the experimental diffusion parameters of Harrison et al., 2009 for the 0.5 mm grain-size*  
 191 *models (the results for the other grain sizes will scale accordingly).*

192

193

194 **Table 2.** *Model results for muscovite diffusion run with cylindrical geometry and at 1*  
 195 *GPa.*

Linear Models		Cooling Rate ( $^{\circ}\text{C}\text{Ma}^{-1}$ )									
		5		10		25		50		70	
Grain Radius	T ( $^{\circ}\text{C}$ )	Time to $0^{\circ}\text{C}$ Ma	$\Delta t$ Ma	Time to $0^{\circ}\text{C}$ Ma	$\Delta t$ Ma	Time to $0^{\circ}\text{C}$ Ma	$\Delta t$ Ma	Time to $0^{\circ}\text{C}$ Ma	$\Delta t$ Ma	Time to $0^{\circ}\text{C}$ Ma	$\Delta t$ Ma
0.25 mm	450	90	2.40	45	0.84	18	0.20	9	0.07	6.4	0.04
	500	100	10.10	50	3.91	20	1.05	10	0.37	7.1	0.23
	600	120	31.26	60	14.45	24	5.13	12	2.31	8.6	1.58
	700	140	52.08	70	24.87	28	9.31	14	4.40	10	3.06
0.5 mm	450	90	1.15	45	0.38	18	0.09	9	0.03	6.4	0.01
	500	100	5.81	50	2.10	20	0.54	10	0.19	7.1	0.12
	600	120	26.45	60	11.96	24	4.10	12	1.78	8.6	1.18
	700	140	47.35	70	22.44	28	8.30	14	3.88	10	2.67
1 mm	450	90	0.52	45	0.16	18	0.03	9	0.01	6.4	0.00
	500	100	2.99	50	1.04	20	0.25	10	0.09	7.1	0.06
	600	120	21.33	60	9.31	24	2.99	12	1.21	8.6	0.76
	700	140	42.29	70	19.82	28	7.20	14	3.32	10	2.26
1/t Models											
Grain Radius	T ( $^{\circ}\text{C}$ )	Time to $0^{\circ}\text{C}$ Ma	$\Delta t$ Ma	Time to $0^{\circ}\text{C}$ Ma	$\Delta t$ Ma	Time to $0^{\circ}\text{C}$ Ma	$\Delta t$ Ma	Time to $0^{\circ}\text{C}$ Ma	$\Delta t$ Ma	Time to $0^{\circ}\text{C}$ Ma	$\Delta t$ Ma
0.25 mm	450	90	0.58	45	0.19	18	0.05	9	0.02	6.4	0.01
	500	100	2.61	50	0.95	20	0.25	10	0.09	7.1	0.05
	600	120	10.27	60	4.60	24	1.56	12	0.67	8.6	0.44
	700	140	18.06	70	8.43	28	3.06	14	1.41	10	0.96
0.5 mm	450	90	0.26	45	0.08	18	0.02	9	0.00	6.4	0.00
	500	100	1.36	50	0.48	20	0.12	10	0.04	7.1	0.03
	600	120	8.12	60	3.52	24	1.13	12	0.46	8.6	0.29

196

	700	140	15.65	70	7.23	28	2.57	14	1.16	10	0.79
1 mm	450	90	0.10	45	0.03	18	0.00	9	0.00	6.4	0.00
	500	100	0.66	50	0.22	20	0.06	10	0.02	7.1	0.01
	600	120	5.97	60	2.45	24	0.70	12	0.26	8.6	0.16
	700	140	13.25	70	6.02	28	2.09	14	0.92	10	0.62

197

198

199

**Table 3.** Model results for muscovite diffusion run with cylindrical geometry and at 2 GPa.

Linear Models		Cooling Rate ( $^{\circ}\text{C}\text{Ma}^{-1}$ )									
		5		10		25		50		70	
Grain Radius	T ( $^{\circ}\text{C}$ )	Time to $0^{\circ}\text{C}$ Ma	$\Delta t$ Ma	Time to $0^{\circ}\text{C}$ Ma	$\Delta t$ Ma	Time to $0^{\circ}\text{C}$ Ma	$\Delta t$ Ma	Time to $0^{\circ}\text{C}$ Ma	$\Delta t$ Ma	Time to $0^{\circ}\text{C}$ Ma	$\Delta t$ Ma
0.25 mm	450	90	0.82	45	0.27	18	0.05	9	0.01	6.4	0.00
	500	100	4.33	50	1.56	20	0.40	10	0.14	7.1	0.09
	600	120	25.22	60	11.29	24	3.80	12	1.62	8.6	1.06
	700	140	47.06	70	22.27	28	8.21	14	3.83	10	2.63
0.5 mm	450	90	0.31	45	0.07	18	0.01	9	0.00	6.4	0.00
	500	100	2.24	50	0.80	20	0.20	10	0.07	7.1	0.04
	600	120	19.86	60	8.52	24	2.64	12	1.04	8.6	0.64
	700	140	41.87	70	19.58	28	7.08	14	3.25	10	2.21
1 mm	450	90	0.05	45	0.01	18	0.00	9	0.00	6.4	0.00
	500	100	1.12	50	0.38	20	0.08	10	0.02	7.1	0.01
	600	120	14.12	60	5.59	24	1.53	12	0.56	8.6	0.34
	700	140	36.32	70	16.69	28	5.87	14	2.62	10	1.76

200

1/t Model s		Cooling Rate ( $^{\circ}\text{C}\text{Ma}^{-1}$ )									
		5		10		25		50		70	
Grain Radius	T ( $^{\circ}\text{C}$ )	Time to $0^{\circ}\text{C}$ Ma	$\Delta t$ Ma	Time to $0^{\circ}\text{C}$ Ma	$\Delta t$ Ma	Time to $0^{\circ}\text{C}$ Ma	$\Delta t$ Ma	Time to $0^{\circ}\text{C}$ Ma	$\Delta t$ Ma	Time to $0^{\circ}\text{C}$ Ma	$\Delta t$ Ma
0.25 mm	450	90	0.16	45	0.04	18	0.01	9	0.00	6.4	0.00
	500	100	0.94	50	0.33	20	0.08	10	0.03	7.1	0.02
	600	120	7.11	60	3.03	24	0.93	12	0.37	8.6	0.23
	700	140	14.68	70	6.75	28	2.39	14	1.07	10	0.73
0.5 mm	450	90	0.04	45	0.01	18	0.00	9	0.00	6.4	0.00
	500	100	0.47	50	0.16	20	0.04	10	0.01	7.1	0.00
	600	120	5.01	60	1.99	24	0.54	12	0.20	8.6	0.12
	700	140	12.32	70	5.58	28	1.92	14	0.84	10	0.56
1 mm	450	90	0.00	45	0.00	18	0.00	9	0.00	6.4	0.00
	500	100	0.21	50	0.06	20	0.01	10	0.00	7.1	0.00
	600	120	3.01	60	1.10	24	0.28	12	0.10	8.6	0.06

	700	140	9.98	70	4.41	28	1.46	14	0.61	10	0.40
--	-----	-----	------	----	------	----	------	----	------	----	------

201

202

203

**Table 4.** Model results for biotite diffusion.

Linear Models		Cooling Rate (°C Ma <sup>-1</sup> )									
		5		10		25		50		70	
Grain Radius	Starting T (°C)	Time to 0°C Ma	Δt Ma	Time to 0°C Ma	Δt Ma	Time to 0°C Ma	Δt Ma	Time to 0°C Ma	Δt Ma	Time to 0°C Ma	Δt Ma
0.25 mm	450	90	25.88	45	11.89	18	4.24	9	1.91	6.4	1.27
	500	100	35.88	50	16.92	20	6.24	10	2.91	7.1	2.00
	600	120	55.88	60	26.92	24	10.24	12	4.91	8.6	3.41
	700	140	75.88	70	36.92	28	14.24	14	6.91	10	4.87
0.5 mm	450	90	21.82	45	9.78	18	3.34	9	1.42	6.4	0.96
	500	100	31.82	50	14.82	20	5.34	10	2.49	7.1	1.63
	600	120	51.82	60	24.82	24	9.34	12	4.49	8.6	3.11
	700	140	71.82	70	34.82	28	13.34	14	6.49	10	4.56
1 mm	450	90	17.45	45	7.54	18	2.39	9	0.96	6.4	0.63
	500	100	27.45	50	12.51	20	4.39	10	1.97	7.1	1.28
	600	120	47.45	60	22.51	24	8.39	12	3.97	8.6	2.77
	700	140	67.45	70	32.51	28	12.39	14	5.97	10	4.21

204

1/t Models		Cooling Rate (°C Ma <sup>-1</sup> )									
Grain Radius	T (°C)	Time to 0°C Ma	Δt Ma	Time to 0°C Ma	Δt Ma	Time to 0°C Ma	Δt Ma	Time to 0°C Ma	Δt Ma	Time to 0°C Ma	Δt Ma
0.25 mm	450	90	11.10	45	4.97	18	1.67	9	0.75	6.4	0.49
	500	100	15.76	50	7.25	20	2.62	10	1.18	7.1	0.80
	600	120	25.13	60	11.85	24	4.42	12	2.08	8.6	1.42
	700	140	34.39	70	16.45	28	6.23	14	2.95	10	2.07
0.5 mm	450	90	8.77	45	3.83	18	1.19	9	0.52	6.4	0.33
	500	100	13.31	50	6.03	20	2.14	10	0.94	7.1	0.63
	600	120	22.31	60	10.45	24	3.83	12	1.76	8.6	1.23
	700	140	31.40	70	14.89	28	5.54	14	2.65	10	1.80

1 mm	450	90	6.45	45	2.64	18	0.7 9	9	0.3 1	6.4	0.19
	500	100	10.8 1	50	4.76	20	1.5 8	10	0.6 9	7.1	0.45
	600	120	19.5 4	60	9.06	24	3.2 4	12	1.4 7	8.6	1.04
	700	140	28.2 8	70	13.3 3	28	4.9 3	14	2.3 6	10	1.58

205

206

The graphs all show similar trends:

207

(1) Faster cooling results in a smaller difference in time between the timing of maximum temperature attainment (cooling initiation) and the recorded cooling age ( $\Delta t$ ).

208

209

(2) Colder initial “peak” starting temperatures result in smaller  $\Delta t$ .

210

(3) Smaller grain sizes result in larger  $\Delta t$ .

211

(4) Smaller  $\Delta t$  values are recorded for the  $1/t$  models than for the linear models.

212

Results (1) and (3) are consistency checks to show that the models are behaving as expected. Result (2) similarly matches the predictions of the modified formulation of Ganguly and Tirone, 1999. Result (4) clearly shows the importance of the cooling path shape on the resulting thermochronometer age – this will be discussed further below.

216

Figure 2 shows that very little diffusive loss is expected in white mica grains that cool from relatively low peak temperatures of 450°C. The  $^{40}\text{Ar}/^{39}\text{Ar}$  age of a 0.25 mm radius white mica grain cooling linearly at a rate of 5°C $\text{Ma}^{-1}$  from 450°C and 1 GPa would be expected to be 2.4 Ma younger than the peak temperature age, whereas one cooling from 700°C would be expected to yield an age that is 52 Ma younger (Table 2). Similarly, the  $^{40}\text{Ar}/^{39}\text{Ar}$  age of a 0.25 mm radius white mica grain cooling linearly at a rate of 5°C $\text{Ma}^{-1}$  from 600°C and 2 GPa would be expected to be ~25 Ma younger than the peak temperature age (Table 3). Similar-sized grains cooling to 0°C over the same time interval but following a  $1/t$  path from 450°C or 700°C at 1 GPa would only yield ages that were 0.6 or 16 Ma younger than the peak temperature age. A 1 mm radius grain cooling from 450°C, however, would be expected to record an age within uncertainty of the timing of peak metamorphism.

227

Models run using spherical diffusion geometry yield slightly younger ages ( $\Delta t$  of 54 Ma rather than 52 Ma for a 0.25 mm radius grain cooling from 700°C at 5°C $\text{Ma}^{-1}$  for example; Supplementary Table S.5; Supplementary Figure S.6).

230

Figure 3 shows that biotite should yield significantly younger ages than muscovite for grains of the same radius, cooling from the same starting temperature and following the same cooling path. For example a 0.25 mm radius grain cooling at 5°C $\text{Ma}^{-1}$  from 450°C would be expected to be 26 Ma younger than the age of peak temperature metamorphism, whereas one

233

234 cooling from 700°C at the same rate would be expected to yield an age that was 76 Ma younger  
235 (Table 3).

236

## 237 **Discussion**

238 The results clearly show that the shape of the cooling path makes an increasingly  
239 important contribution to the recorded thermochronometer age as grain sizes and cooling rates  
240 decrease and peak temperatures increase. The uncertainty inherent in using the Dodson  $T_c$   
241 formulation to estimate (linear) cooling rates therefore also magnifies accordingly.

242 The model results are more sensitive to systematic uncertainties in the experimentally-  
243 determined activation energy ( $E_a$ ) than in the exponential pre-factor ( $D_0$ ) for each mineral  
244 (Figures 2-4 and Supplementary Table S.7). These figures show that uncertainties in the  
245 diffusion parameters have a significant, but systematic, effect on the recorded  
246 thermochronological ages. These uncertainties apply equally to both cooling history shapes  
247 discussed here.

248 The most recent diffusion parameters for muscovite (Harrison et al., 2009) were  
249 calculated for isotropic 3-dimensional (spherical) diffusion geometry. It has been suggested  
250 that modelling muscovite as a cylinder but using diffusion parameters calculated for spherical  
251 geometry invalidates the results (Foster and Lister, 2017). However the overall difference in  
252 the diffusion coefficient is a factor 2 in  $D_0$ , which translates into an activation barrier of <0.6  
253 kcal/mol at 400 K. This is well below the uncertainty of 7 kcal/mol in the Harrison et al., 2009  
254 diffusion parameters and thus adds no extra uncertainty to our overall results, as also suggested  
255 in other studies (e.g. Huber et al., 2011).

256

## 257 **Applying Model Results to Natural Systems**

258 The results presented here can be used to constrain the cooling rates of natural  
259 systems if the following pieces of information are known or can be estimated:

260 1) A petrographically-based interpretation of the temperature at which the dated  
261 grain(s) grew, and the portion of the metamorphic path along which the grain(s) grew (e.g.  
262 prograde peak or retrograde). This will inform and constrain the extent of diffusive opportunity  
263 that the grain could have experienced. For example a grain growing during the prograde history  
264 will have longer residence at high temperatures, therefore allowing it more opportunity to lose  
265 argon.

266 2) The peak temperature experienced by the grain(s), required for the ultimate  
267 determination of a cooling rate.



268 3) The time at which the grain reached its peak temperature (constrained or estimated  
269 by independent geochronometers), required for the ultimate determination of a cooling rate.  
270 This is further discussed below.

271 4) The thermochronometric ages of the grains of interest; different data collection  
272 methods are further discussed below.

273 5) The grain size(s) of the dated grains.

274 6) The assumption or knowledge that open grain-boundary, thermally-activated  
275 diffusion was the dominant process in determining the final Ar concentration. This  
276 approximation is difficult to assess (e.g. Warren et al., 2012a,b) but should be acknowledged  
277 in any thermochronological interpretation.

278 Note that only very simple cooling path shapes have been modelled here. Steady  
279 progress is being made in the development of modelling tools that can suggest a “best fit”  
280 cooling path to U-Th-He, fission track and U-Pb rutile data, but currently none of these tools  
281 explicitly incorporate  $^{40}\text{Ar}/^{39}\text{Ar}$  data: e.g. HeFTy (Ketcham, 2005), QTQt (Gallagher, 2012),  
282 UpBeat (Smye et al., 2018).

283

284 **Determining the timing of cooling initiation:** Direct determination of a cooling rate  
285 (and cooling rate shape) from thermo- and geochronological data requires that at least two, and  
286 possibly three, T-t pairs are known. Timing of peak T in metamorphic rocks is commonly  
287 constrained by U-Pb ages of zircon, monazite, garnet, allanite and/or rutile, with secondary  
288 (higher-temperature cooling) T-t pairs provided by U-Pb rutile and/or titanite data. There are,  
289 of course, multiple uncertainties inherent in linking these ages to peak temperature because all  
290 of these minerals may crystallise at different stages of the metamorphic PT path. Careful  
291 petrochronological investigation is required to confirm that the ages yielded by any of these  
292 minerals relate to the timing of attainment of peak temperatures or higher-than-argon-closure  
293 cooling (e.g. Kohn et al., 2017).

294

295  **$^{40}\text{Ar}/^{39}\text{Ar}$  data collection methods:**  $^{40}\text{Ar}/^{39}\text{Ar}$  mica data can currently be collected in  
296 many different ways: by multiple- or single-grain step heating experiments (e.g. Turner, 1970),  
297 by single grain fusion methods (e.g. Fleck and Carr, 1990) or by laser ablation (e.g. Kelley et  
298 al., 1994). All methods have their advantages and disadvantages in terms of volume of material  
299 analysed, analytical precision and petrographic (location) control on age.

300 The model data presented here are compatible for assessment against the bulk (volume-  
301 averaged) ages – i.e. equivalent to single grain fusion  $^{40}\text{Ar}/^{39}\text{Ar}$  data. We caution against using  
302 multiple-or single-grain step heating  $^{40}\text{Ar}/^{39}\text{Ar}$  ages to compare against model results. Plateau

303 ages imply no core-rim variation in Ar distribution, (and thus an interpretation of rapid  
304 cooling), but a plateau result does not in itself guarantee that the calculated age is geologically  
305 meaningful, especially in high pressure metamorphic rocks (e.g. Sherlock and Arnaud, 1999).  
306 Non-plateau spectra can be produced by a variety of factors that complicate linking spectrum  
307 shapes to within-grain Ar distribution. Single grain fusion populations can help provide an  
308 assessment of how homogeneous Ar is distributed across mica grains within individual samples  
309 (e.g. Uunk et al., 2018).

310 In-situ, high-spatial precision  $^{40}\text{Ar}/^{39}\text{Ar}$  data such as collected by laser ablation  
311 methods, and collected in grains large enough and cooled slowly enough from a high enough  
312 temperature to be able to detect such changes, can also be assessed against the core-rim model  
313 age predictions for simple linear and  $1/t$  cooling histories presented in Supplementary Tables  
314 S.2 -S.4.

315

316 **Comparing analytical data to model results:** The time difference ( $\Delta t$ ) between the  
317 timing of the thermal peak (or to be absolutely correct, the timing of cooling initiation) and the  
318 age recorded by the thermochronometer (Figures 2-4 ) provides a basis for determining cooling  
319 rates under the fundamental approximations (1) that thermally activated volume diffusion was  
320 the only mechanism by which the daughter isotope was mobilised within the mineral; (2) that  
321 the mineral crystallized with no inherited daughter isotope; and (3) that the experimentally-  
322 derived diffusion parameters mimic what happens in nature. It is important to acknowledge  
323 that minerals may not degas in a high-vacuum environment in an experiment that lasts a few  
324 days in the same way that a mineral degasses in a rock over millions of years, however these  
325 experimental data are the best available at the present day.

326 For example, consider a scenario whereby a 0.5 mm radius muscovite in a rock that  
327 started cooling from 500°C at 100 Ma yields an age of 94 Ma.  $\Delta t$  is therefore 6 Ma. Table 2  
328 and Figure 2 suggest that those data are compatible with a linear cooling rate of 5°C/Ma<sup>-1</sup>.  
329 However this is not enough information to determine whether (a) the system was diffusively  
330 open (a fundamental requirement of any diffusive-based interpretative link between age,  
331 temperature and cooling rate is that effectively there is infinite sink for the daughter element  
332 diffusing out of the mineral grain) and/or (b) whether the cooling path was overall linear or  
333 some other shape. Both of these can be resolved following a match between data and model  
334 predictions.

335 For example, a rock cooling from 600°C might yield 1 mm radius biotite grains with a  
336  $\Delta t$  of 9 Ma, 0.5 mm radius grains with a  $\Delta t$  of 10.5 Ma and 0.25 mm radius grains with a  $\Delta t$  of  
337 12 Ma. These data would be compatible with a cooling path of  $1/t$  shape that cooled to 0°C

338 over 60 Ma. A minimum of two different ages – either different grain sizes of the same mineral  
339 or different minerals, should allow differentiation of the best-fit cooling path.

340 At rapid cooling rates, the difference between the cooling ages predicted by a linear  
341 temperature decrease and a 1/t-shaped path would be indistinguishable within the typical  
342 uncertainties in analytical results and in the experimental diffusion parameters. At cooling  
343 rates  $<10^{\circ}\text{C}\text{Ma}^{-1}$ , differences in the shapes of the cooling paths start to become important for  
344 distinguishing between exhumation mechanisms.

345 Small values of  $\Delta t$  e.g.  $< 1$  Ma are currently challenging to resolve analytically. The  
346 mica  $^{40}\text{Ar}/^{39}\text{Ar}$  models for low starting temperatures confirm previous suggestions that rapidly-  
347 cooled rocks that reached low peak temperatures (such as in subduction zones) will not yield  
348 ages that allow cooling rates to be determined.

349

350 **Other factors affecting daughter element distribution:** Inheritance or loss of  
351 daughter product during recrystallization and deformation during cooling can affect daughter  
352 element concentrations much more than diffusion (Villa 1998; Allaz et al., 2011; Villa et al.,  
353 2014). It is also obvious that re-crystallisation during exhumation means that the temperature  
354 that that particular grain cooled from may be lower than the peak temperature. In cases where  
355 thermochronometer minerals show signs of secondary recrystallization or other chemical  
356 modification, the model results are almost certainly not applicable, and a link between  
357 temperature and age may be more difficult to constrain. The diffusion models are *only*  
358 applicable to rocks in which an open system can be assumed, and where both the timing and  
359 pressure-temperature conditions of the last episode of mineral crystallisation are known or can  
360 be estimated.

361 If the results presented here are used to estimate cooling rates or constrain cooling path  
362 shapes, each practitioner will need to estimate the geological uncertainty for their particular  
363 study, noting that this is almost certainly the largest overall source of error in their  
364 interpretation. Our results are based on the assumption that cooling starts directly after the  
365 model grain has crystallised at peak temperatures. In reality, the minerals of interest may have  
366 grown along the prograde path and/or have resided at peak temperatures for a geologically-  
367 significant period of time before cooling started. If temperatures were low enough for diffusion  
368 to be inefficient, some of that pre-cooling history may be recorded in the thermochronometer  
369 minerals. Thermochronologists should model the effect of pre-peak thermal history for their  
370 particular geological location to convince themselves whether or not the thermochronometer  
371 minerals in their study area may record this.

372

373  
374  
375  
376  
377  
378  
379  
380  
381  
382  
383  
384  
385  
386  
387  
388  
389  
390  
391  
392  
393  
394  
395  
396  
397  
398  
399  
400  
401  
402  
403  
404  
405  
406

## Conclusions

The rates and timescales over which rocks are buried, transformed, deformed and exhumed help constrain the tectonic mechanisms that act on them.  $^{40}\text{Ar}/^{39}\text{Ar}$  data from micas have long been used to link time to temperature and thus constrain cooling rates. The Dodson closure temperature formulation (Dodson, 1973) provides an elegant analytical solution to the diffusion equation but its application for determining cooling rates is commonly based on assumptions that are a poor match to geological reality. Our results of a series of diffusion models that quantify the differences in age expected from a simple linear and  $1/t$ -shaped cooling histories show that the cooling path shape exerts considerable influence on the resulting age at hotter starting temperatures, slower cooling rates and smaller grain sizes. If the cooling path shape and timing of cooling initiation are known, then our results also provide a simple way of estimating cooling rates and cooling rate shapes from the difference between the timing of cooling initiation at maximum temperature and the yielded thermochronometer age. Future incorporation of  $^{40}\text{Ar}/^{39}\text{Ar}$  diffusion systematics into forward modelling packages that also incorporate other thermochronometers provides the best future solution for constraining cooling rates, with the caveat that more precise diffusion data are needed.

## Acknowledgements

CSM was funded on an Open University Charter Studentship. CJW acknowledges prior financial support from a NERC Advanced Fellowship (NE/H016279/1) and a NERC small grant (NE/J013072/1). The authors thank Simon Kelley for many fruitful discussions about linking age to stage and open system behaviour, and Leo Ingvorsen for helping to run some of the early models. CSM thanks Sarah Sherlock and Alison Halton for PhD supervision and guidance.

## References

- Allaz, J., Engi, M., Berger, A. & Villa, I. 2011. The Effects of Retrograde Reactions and of Diffusion on  $^{40}\text{Ar}/^{39}\text{Ar}$  Ages of Micas. *Journal of Petrology*, 52, 691–716, doi: 10.1093/petrology/egq100.
- Condon, D. J. & Schmitz, M. D. One hundred years of isotope geochronology, and counting. *Element*, 9. 15-17, doi: 10.2113/gselements.9.1.15.

407 Dodson, M. H. 1973. Closure temperatures in cooling geological and petrological systems.  
408 Contrib. Mineral. Petrol., 40, 259–274, doi: 10.1007/BF00373790.

409 Fleck, R.J. and Carr, M.D., 1990. The age of the Keystone Thrust: Laser-fusion  $^{40}\text{Ar}/^{39}\text{Ar}$   
410 dating of Foreland Basin Deposits, southern Spring Mountains, Nevada. *Tectonics*, 9,  
411 467-476.

412 Forster, M. A. & Lister, G. S. 2017,  $^{40}\text{Ar}/^{39}\text{Ar}$  geochronology and the diffusion of  $^{39}\text{Ar}$  in  
413 phengite-muscovite intergrowths during step-heating experiments in vacuo. In Jourdan,  
414 F., Mark, D. F. & Verati, C. (eds) 2014. *Advances in  $^{40}\text{Ar}/^{39}\text{Ar}$  Dating: from*  
415 *Archaeology to Planetary Sciences*. Geological Society, London, Special Publications,  
416 378, 117–135, doi: 10.1144/SP378.16.

417 Gallagher, K., 2012. Transdimensional inverse thermal history modeling for quantitative  
418 thermochronology. *J. Geophys. Res. Solid Earth*, 117, doi: 10.1029/2011JB008825

419 Ganguly J, Tirone M. 1999. Diffusion closure temperature and age of a mineral with arbitrary  
420 extent of diffusion: theoretical formulation and applications. *Earth and Planetary*  
421 *Science Letters*, 170, 131-40.

422 Ganguly J, Tirone M. 2009. Closure temperature, cooling age and high temperature  
423 thermochronology. In: *Physics and Chemistry of the Earth's Interior* (pp. 89-99).  
424 Springer, New York, NY.

425 Hames, W. E. & Bowring, S. A. 1994. An empirical evaluation of the argon diffusion geometry  
426 in muscovite. *Earth and Planetary Science Letters*, 124, 161–167, doi:10.1016/0012-  
427 821X(94)00079-4.

428 Harrison, T. M., Duncan, I. & McDougall, I. 1985. Diffusion of  $^{40}\text{Ar}$  in biotite: Temperature,  
429 pressure and compositional effects. *Geochimica et Cosmochimica Acta*, 49, 2461-2468,  
430 doi: 10.1016/0016-7037(85)90246-7.

431 Harrison, T. M., Celerier, J., Aikman, A. B., Hermann, J. & Heizler, M. T. 2009. Diffusion of  
432  $^{40}\text{Ar}$  in muscovite. *Geochim. Cosmochim. Act.*, 73, 1039-1051, doi:  
433 10.1016/j.gca.2008.09.038.

434 Huber, C., Cassata, W.S. & Renne, P.R. 2011. A lattice Boltzmann model for noble gas  
435 diffusion in solids: The importance of domain shape and diffusive anisotropy and  
436 implications for thermochronometry. *Geochim. Cosmochim. Act.*, 8, 2170-2186.  
437 doi:10.1016/j.gca.2011.01.039.

438 Kelley, S. P., Arnaud, N. O., and Turner, S. P., 1994. High spatial resolution  $^{40}\text{Ar}/^{39}\text{Ar}$   
439 investigations using an ultra-violet laser probe extraction technique. *Geochim.*  
440 *Cosmochim. Act.*, 58, 3519-3525.

441 Ketcham, R.A., 2005. Forward and inverse modeling of low-temperature thermochronometry  
442 data. *Rev. Mineral. Geochem.*, 58, 275-314.

443 Kohn, M.J., Engi, M., Lanari, P. (eds), 2017. *Petrochronology: Methods and Applications*.  
444 *Reviews in Mineralogy* 83, pp 575. ISBN 978-0-939950-05-8

445 Mark, D. M., Kelley, S. P., Lee, M. R., Parnell, J., Sherlock, S. C. & Brown, D. J., 2008. Ar-  
446 Ar dating of authigenic K-feldspar: Quantitative modelling of radiogenic argon-loss  
447 through subgrain boundary networks. *Geochimica et Cosmochimica Acta*, 72, 2695-  
448 27100, doi: 10.1016/j.gca.2008.03.018.

449 McDonald, C. S., Warren, C. J., Mark, D. F., Halton, A. M., Kelley, S. P. & Sherlock, S. C.,  
450 2016. Ar redistribution during a metamorphic cycle: Consequences for determining  
451 cooling rates. *Chemical Geology*, 443, 182-197, doi: 10.1016/j.chemgeo.2016.09.028.

452 Reiners, P. W., 2005. Past, Present, and Future of Thermochronology. *Reviews in Mineralogy*  
453 *and Geochemistry*. 58: 1. doi:10.2138/rmg.2005.58.1

454 Sherlock, S.C. and Arnaud, N.O., 1999. Flat plateau and impossible isochrons: Apparent  $^{40}\text{Ar}$ -  
455  $^{39}\text{Ar}$  geochronology in a high-pressure terrain. *Geochimica et Cosmochimica Acta*, 63,  
456 2835-2838.

457 Smye, A.J., Marsh, J.H., Vermeesch, P., Garber, J.M., Stockli, D.F., 2018. Applications and  
458 limitations of U-Pb thermochronology to middle and lower crustal thermal histories.  
459 *Chemical Geology* 494, 1-18. doi: 10.1016/j.chemgeo.2018.07.003

460 Turner, G., 1970.  $^{40}\text{Ar}/^{39}\text{Ar}$  age determination of lunar rock 12013. *Earth and Planetary*  
461 *Science Letters*, 9, 177-180.

462 Uunk B, Brouwer F, ter Voorde M, Wijbrans J., 2018. Understanding phengite argon closure  
463 using single grain fusion age distributions in the Cycladic Blueschist Unit on Syros,  
464 Greece. *Earth and Planetary Science Letters*, 484, 192-203.

465 Villa, I. M., 1998. Isotopic Closure. *Terra Nova*, 10, 42-47, doi: 10.1046/j.1365-  
466 3121.1998.00156.x

467 Villa, I. M., Bucher, S., Bousquet, R., Kleinhanns, I. C. & Schmid, S. M., 2014. Dating  
468 polygenetic metamorphic assemblages along a transect across the western Alps. *Journal*  
469 *of Petrology*, 55, 803–830, doi: 10.1093/petrology/egu007.

470 Warren, C. J., Hanke, F. & Kelley, S. P. 2012a. When can muscovite  $^{40}\text{Ar}/^{39}\text{Ar}$  dating constrain  
471 the timing of metamorphic exhumation? *Chemical Geology*, 291, 79–86, doi:  
472 10.1016/j.chemgeo.2011.09.017.

473 Warren, C. J., Kelley, S. P., Sherlock, S. C. & McDonald, C. S. 2012b. Metamorphic rocks  
474 seek meaningful cooling rate: Interpreting  $^{40}\text{Ar}/^{39}\text{Ar}$  ages in an exhumed ultra-high  
475 pressure terrane. *Lithos*, 155, 30-48, doi: 10.1016/j.lithos.2012.08.011.

- 476 Wartho, J. A., Kelley, S. P. & Elphick, S. C. 2013. Ar diffusion and solubility measurements  
477 in plagioclase using ultra-violet laser depth-profiling techniques. Geological Society,  
478 London, Special Publications, 378, 137-154, doi: 10.1144/SP378.13.
- 479 Wheeler, J. 1996. DIFFARG: A program for simulating argon diffusion profiles in minerals.  
480 Computers and Geosciences, 22, 919–929, doi: 10.1016/S0098-3004(96)00061-1.

481  
482

## 483 **Supplementary Data**

484

485 **S.1** Instructions for operating DiffargP\_inverse

486

487 **S.2** Full muscovite results for 1GPa models

488

489 **S.3** Full muscovite results for 2GPa models

490

491 **S.4** Full biotite model results

492

493 **S.5.** Full muscovite results for spherical geometry models

494

495 **S.6.** Muscovite linear and 1/t results for models run at 1 GPa with spherical geometry.

496 Different coloured lines show different grain sizes. A-D show results for linear models at  
497 different starting temperatures; E-H show results for 1/t models that run over the same  
498 timescale. For ease of comparison, both sets of models run for the equivalent “time to surface”  
499 which is plotted on the *x*-axis. The equivalent linear rate is plotted underneath the “time to  
500 surface” value on the linear model plots. The *y*-axis plots the difference between the time at  
501 which cooling starts and the recorded <sup>40</sup>Ar/<sup>39</sup>Ar age: if this is, the grain size and the starting  
502 temperature are known for the analysed samples, then the cooling rate can be read off the graph  
503 directly. Note the differences in the *y*-axis scale between the linear and 1/t results.

504

505 **S.7.** Results of sensitivity tests

506

507

508

509

510